Int J Adv Manuf Technol (2015) 81:2017–2026
DOI 10.1007/s00170-015-7332-7

ORIGINAL ARTICLE

Material removal mechanism of cluster magnetorheological effect in plane polishing

Jisheng Pan [1] · **Qiusheng Yan** [1]

Received: 11 December 2014 / Accepted: 15 May 2015 / Published online: 3 June 2015
© Springer-Verlag London 2015

Abstract A cluster magnetorheological (MR) plane polishing based on a combination of magnetorheological finishing (MRF) and cluster mechanism (arrange in a regular array) has been developed for large planar optical workpiece. In this paper, the polishing pressure of an individual MR micro-grinding head on workpieces was investigated, and the mathematical model for cluster MR plane polishing was established based on the Preston equation and the properties of the workpiece material. An arc-shaped polishing belt was processed on monocrystalline 6H-SiC and Si wafer by the cluster MR polishing apparatus which polishing disk inlaid with cylindrical flat bottom magnetic pole arrange in the same direction regularly and monocyclically. The profile of arc polishing belt's cross section and the surface morphology were observed and analysed to verify the obtained model. The abrasives with different size were found to have an equal effect on the processed surface because of the accommodated-sinking effect of the polishing pad constituted by the cluster MR micro-grinding head. It was found that the monocrystalline 6H-SiC and Si wafer were polished in a plastic mode with a smooth, damage-free surface.

Keywords Cluster MR effect · Material removal mechanism · Polishing pressure · Semi-fixed abrasive

✉ Jisheng Pan
panjisheng@gdut.edu.cn

[1] Guangdong University of Technology, Guangzhou, China

1 Introduction

Magnetorheological finishing (MRF) is a novel optical surface processing method combining electromagnetics, fluid dynamics, analytical chemistry, processing technology, which was proposed by Kordonski in the 1990s [1]. Comparing to the traditional polishing, MRF abrasive is constantly delivered to the polishing zone, and polishing debris and heat are continuously removed. This method has been accepted as an effective optical surface machining method [2]. MRF is regarded as a deterministic optical element processing technology because the availability of the material removal volume can be measured by optical interferometer. Sidpara et al. proposed a theoretical model of forces acting on the workpiece in MR fluid-based finishing process and carried out an experimental investigation to measure the forces on the freeform surface. The effect of size, concentration and type of abrasive particles as well as the size of magnetic particles on material removal rate and surface roughness of single crystal silicon were also investigated [3–5]. Sidpara and Li et al. made some nano level finishing for semiconductor materials using magnetorheological finishing process and optimised the values of process parameters [6, 7]. Some different mathematical models of material removal in MRF were proposed [8–10]. Also, some new process methods such as ball end magnetorheological finishing (BEMRF) process [11, 12], magnetorheological abrasive flow finishing (MRAFF) process [13, 14] and magnetic compound fluid slurry (MCF) polishing [15, 16] were developed in recent years.

When processing a planar workpiece with MRF, the polishing belt and the workpiece surface were contacted in

spot-form. Therefore, the whole surface can only be achieved through controlling the scanning of MRF spot along the workpiece surface in certain regular trajectory. The material removal rate is low and the flatness is difficult to be achieved. Therefore, based on the MRF principle and cluster mechanism (arrange in a regular array), a cluster MR plane polishing method with a high and distributed magnetic field formed by numerous arrays magnets was proposed [17]. Under the influence of a magnetic field, a viscoplastic MR pad is formed between the surface of polishing plate and workpiece. The abrasives are gripped and aggregated on the top of MR pad. The abrasives with different sizes aggregate on the top of MR pad are all equally effective in removing the material while interacting with the machined surface. A large region planarization and smooth surface can be achieved with this method, and a large number optimization study was carried out for difference materials [18, 19].

2 Material removal model of cluster MR plane polishing

2.1 Principle of cluster MR effect polishing

In Fig. 1, the principle of cluster MR plane polishing is illustrated. Small magnetic bodies are embedded on the polishing disk which is made of diamagnetic materials according to the clustering principle. The MR fluid mixed with abrasives reach to the polishing disk surface, the upper part of the magnetic bodies form a chain structure along the direction of the magnetic field lines. With the solidification of this chain structure, the Bingham viscoelastic micro-grinding head with semi-fixed abrasive is formed. The polishing pad is constituted by the micro-grinding heads in a regular array. In the polishing, the abrasive grains present on the contact surface with the workpiece under the normal and shear forces to remove the surface material of the workpiece. Since the semi-fixation of the viscoelastic MR fluid on the abrasive grains is a soft constraint, the surface material of the workpiece is removed flexibly, which can obtain the damage-free ultra-smooth surface with the high efficiency [20, 21].

2.2 Material removal model of cluster MR plane polishing

Yi et al. suggested the MR fluid change the state under three critical magnetic fields strength $Hc1$,$Hc2$, and $Hc3$[22, 23]. When magnetic fields strength $H<Hc1$, the MR fluid was in a fluid state, and the ferromagnetic grains were randomly distributed. When $Hc1<H<Hc2$, the ferromagnetic grains formed a randomly distributed magnetic chains structure that coexisted with the grains. When $Hc2<H<Hc3$, the ferromagnetic grains constituted a columnar structure that coexisted with the chains, and when $H>Hc3$, the ferromagnetic grains formed a columnar structure. The finite element simulation of the magnetic field of a cluster MR disk (Fig. 2a) shows the boundaries of the critical field [20]. Thus, it can be considered that the region $H>Hc2$, the Bingham viscoelastic micro-grinding head was formed.

On the basis of the aforementioned processing principle, the model of cluster MR plane polishing was simplified as follow. It is assumed that the working plane of workpiece and polishing disk are paralleled, the diameter of magnet pole is d, the central distance from the workpiece to the polishing disk is a, the height of the viscoelastic micro-grinding head is h_r, and the gap between the workpiece and polishing disk is h_1. It is assumed that when the workpiece is fixed, the polishing disk move along the X-direction, the Cartesian coordinate system shown in Fig. 2b can be established.

Cluster MR plane polishing is achieved when exerting a pressure by the Bingham viscoelastic micro-grinding head. Then, using the semi-fixed abrasives, the material on the workpiece surface is removed. The process can be expressed using the Preston equation [24]. The mean removal rate (MRR) of the material is given by:

$$\mathrm{MRR} = Kpv \tag{1}$$

where K is the Preston coefficient; under the fixed processing conditions, it is constant. p is the pressure of the MR fluid on

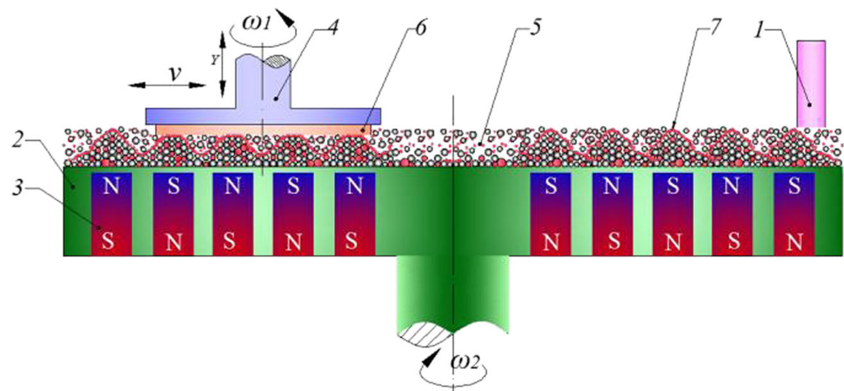

Fig. 1 Principle of cluster MR plane polishing. *1* Working liquid cycle system, *2* polishing disk made by diamagnetic material, *3* cluster magnets, *4* workpiece spindle, *5* MR fluid, *6* workpiece, *7* micro-grinding head

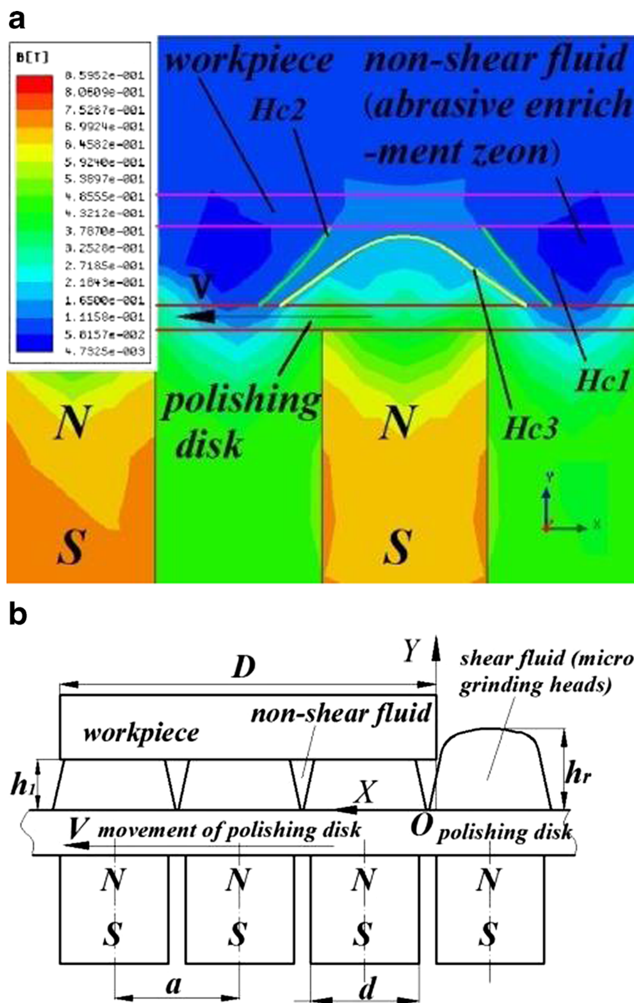

Fig. 2 Diagram of cluster MR plane polishing. **a** Diagram of micro-grinding head (simulated by Maxwell 3D, magnets type: N35 cylindrical flat permanent magnets; magnets dimensions: ϕ10 mm× 20 mm;). **b** Diagram of polishing process

the workpiece, and v is the speed of the MR fluid in the polishing region relative to the workpiece surface.

Buijs et al. [25, 26] proposed that there is the proportional relationship (see Eq. (2)) between the material removal rate and Young's modulus E, hardness H_v and fracture toughness K_c. Therefore, it was necessary to introduce a workpiece material correction coefficient into the material removal model here.

$$K_w = \frac{E^{5/4}}{K_c H_v^2} \tag{2}$$

The polishing pressure p from the micro-grinding head on workpiece is a complex parameter. It is mainly composed of the dynamic pressure of the fluid, the pressure produced by the MR effect, and the buoyancy of the fluid. The pressure generated by the MR effect includes magnetisation and magnetostriction pressures. Since MR fluids are incompressible, the magnetostriction pressure induced by the volume change in the magnetic field is approximately zero. Thus, the polishing pressure can be expressed as:

$$p = p_d + p_g + p_m \tag{3}$$

where p_d is the dynamic pressure of the MR fluid; p_m is the MR pressure; and p_g is the buoyancy of MR fluid. But p_g is much less than p_d and p_m, so it was ignored in the calculation.

2.2.1 The MR pressure of the micro-grinding head on workpiece surface

Zhangfeng et al. [27] proposed that the MR pressure produced by the spherical magnetic particles in the MR fluid under the effect of an external magnetic field was given by:

$$p_m = \frac{3\varphi\mu_0(\mu - \mu_0)}{\mu + 2\mu_0}\int_0^H H dH \tag{4}$$

where μ_0 is the vacuum permeability, H is the strength of the external magnetic field on the workpiece surface, μ is the magnetoconductivity of the magnetic particles, and φ is the proportion of magnetic particles in the MR fluid. The MR pressure is proportional to the strength H of the external magnetic field on the workpiece surface when $H$is greater than $Hc1$. Since the micro-grinding head has an equal probability of acting on each area on the workpiece, the mean of the MR pressure produced thereby is used to approximate the real MR pressure applied by cluster MR effect on the fixed region of a workpiece.

Since the time of a single micro-grinding head passes through a certain point on the workpiece surface is $T=a/v$, so the mean MR pressure can be expressed by the Eq.(5):

$$\overline{p_m} = \frac{v}{a}\sum_{-\frac{a}{2}}^{\frac{a}{2}}\frac{3\varphi\mu_0(\mu - \mu_0)}{\mu + 2\mu_0}\int_0^H H dH \tag{5}$$

2.2.2 The hydrodynamic pressure of the micro-grinding head on the workpiece

The hydrodynamic pressure on the entrance of workpiece As a micro-grinding head moves from $x=-a/2$ to $x=0$, dynamic pressure was produced on the entrance of the workpiece due to the sudden height change of the micro-grinding head. The pressure satisfies Eq. (6) [28]:

$$\frac{dp_d}{dx} = 6\eta v\frac{h - h_0}{h^3} \tag{6}$$

where η is the initial viscosity of the MR fluid, h refers to the height of the micro-grinding head, and h_0 is the distance from the workpiece surface to the polishing disk when $dp_d/dx=0$.

Since the workpiece is parallel to the polishing disk during the cluster MR process, dynamic pressure p_d cannot be obtained according to the Reynolds equation, that is, $dp_d/dx=0$. Therefore, $h_0=h_1$. As a result:

$$\frac{dp_d}{dx} = 6\eta v\frac{h-h_1}{h^3} \tag{7}$$

As shown in Fig. 2a, the height of the micro-grinding head is closely correlated with the magnetic field intensity H. Hence, the dynamic pressure equation is the function of the height h of the micro-grinding head. In accordance with the marginal effect of each pole, h is 0 when the micro-grinding head lies in region $\pm a/2$. Thus, it is hypothesised that $h=h_r$ when the micro-grinding head is in region $-d/2\sim d/2$. Moreover, only when the micro-grinding head is in region $-d/2\sim d/2$, it can exert dynamic pressure on the workpiece. The dynamic pressure is calculated by:

$$p_d = 6\eta v\frac{h_r-h_1}{{h_r}^3} \tag{8}$$

Therefore, the mean of the dynamic pressure generated by the micro-grinding head on the workpiece margin is:

$$\overline{p_d} = 6\eta v\frac{h_r-h_1}{{h_r}^3}\frac{d}{a} \tag{9}$$

The dynamic pressure on other regions of the workpiece When moving below the workpiece, the micro-grinding head lies parallel to the polishing disk. Theoretically, dynamic pressure p_d is not formed in these conditions. As shown in Fig. 2a, if the solid micro-grinding head formed when $H>Hc2$. There would be a new small gap between the upper surface of the solid and the workpiece surface as the MR fluid in the non-shearing region reaches the micro-grinding head region. In this gap, MR fluid moves into the micro-grinding head and applies a dynamic pressure. However, the MR fluid in the non-shearing region is rich of abrasives instead of continuous fluid. In addition, the magnetic chains that form the micro-grinding head would incline in moving. Thus, the dynamic pressure produced can be ignored. It is considered that the MR fluid in the non-shearing region played a role of renewing abrasives on the micro-grinding head [17].

2.2.3 The material removal model

According to the analysis above, the material removal model of the cluster MR effect on a workpiece was established:

$$MRR = \begin{cases} K\cdot\frac{E^{5/4}}{K_cH_v^2}\cdot v\cdot\left(6\eta v\frac{h_r-h_1}{{h_r}^3}\frac{d}{a}+\frac{v}{a}\sum_{-\frac{a}{2}}^{\frac{a}{2}}\frac{3\varphi\mu_0(\mu-\mu_0)}{\mu+2\mu_0}\int_0^H HdH\right) & x=0 \\ K\cdot\frac{E^{5/4}}{K_cH_v^2}\cdot\frac{v^2}{a}\sum_{-\frac{a}{2}}^{\frac{a}{2}}\frac{3\varphi\mu_0(\mu-\mu_0)}{\mu+2\mu_0}\int_0^H HdH & x>0 \end{cases} \tag{10}$$

The coefficient K in Eq. (10) can be obtained by experiment. Subsequently, giving a fixed MR fluid and the magnetic pole arrangement, the material removal rate can be calculated. Therefore, the cluster MR plane polishing is a deterministic polishing processing method.

There are bumps on the workpiece surface, as shown in Fig. 3. Due to the smaller gap between the bumps on the workpiece surface and the polishing disk, the magnetic field strength of bumps is higher than the smooth surface. Thus, the rigidity of the micro-grinding head increases. In addition, the the buoyancy of the micro-grinding head over any bumps also exceeds that on plane. Moreover, the sudden changes of the micro-grinding head induce a new dynamic pressure in the fluid as it passes through bumps. As a result, the material removal rate is far higher on bumps than that on the plane. That is to say, cluster MR plane polishing gives a priority of material removal for the bumps on the workpiece and thus accelerates the flattening of the workpiece.

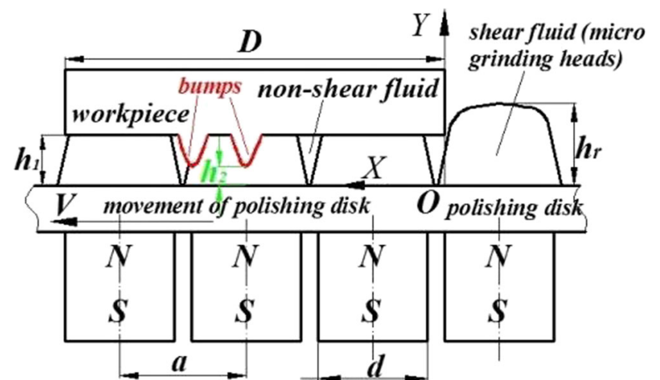

Fig. 3 Material removal model of bumps on workpiece

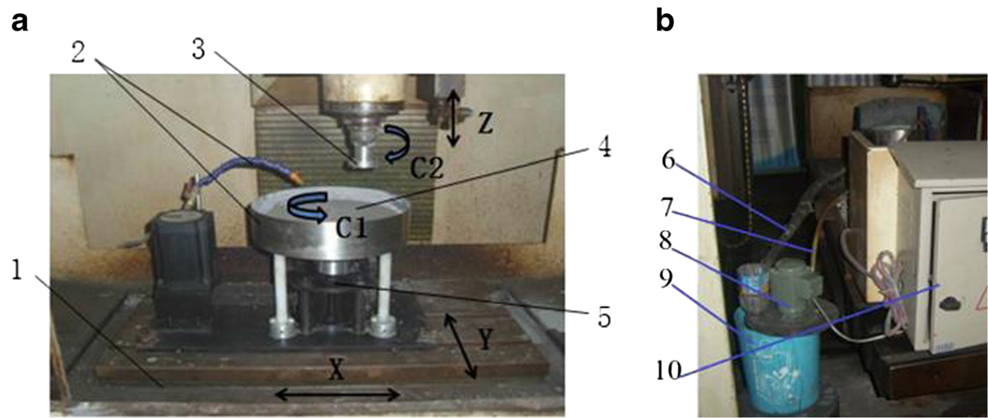

Fig. 4 Experimental apparatus for cluster MR plane polishing. *1* CNC milling machine, *2* working liquid recycle system, *3* workpiece clamping apparatus, *4* rotating polishing disk, *5* magnetic field adjustment apparatus, *6* return pipe, *7* supply pipe, *8* re-circulating pump with mechanical blending, *9* container, *10* electric cabinet. **a** Experimental apparatus and **b** cycle system

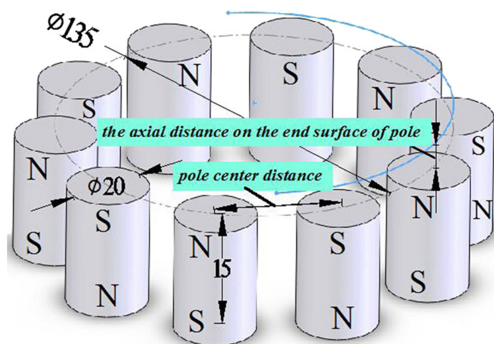

Fig. 5 Diagram of magnetic ring arrangement

3 Experiments and discussion

3.1 Experimental method

To analyse the correctness of the material removal model, a cluster MR plane polishing experimental apparatus was modified on a numerically controlled milling machine, as shown in Fig. 4. This apparatus was used to control the four movements: X, Y, C1 and C2. The MR fluid used in the experiment is composed of 4 % carbonyl iron powder, 88 % deionised water, 4 % abrasives (the abrasive for 6H-SiC is diamond powder, the abrasive for Si is alumina) and 4 % stabiliser. The N35 cylindrical flat permanent magnets with the diameter of 20 mm and the height of 15 mm were synthetically and monocyclically allocated on the 5-mm-thick polishing disk as shown in Fig. 5. The 6H-SiC monocrystalline wafer and the

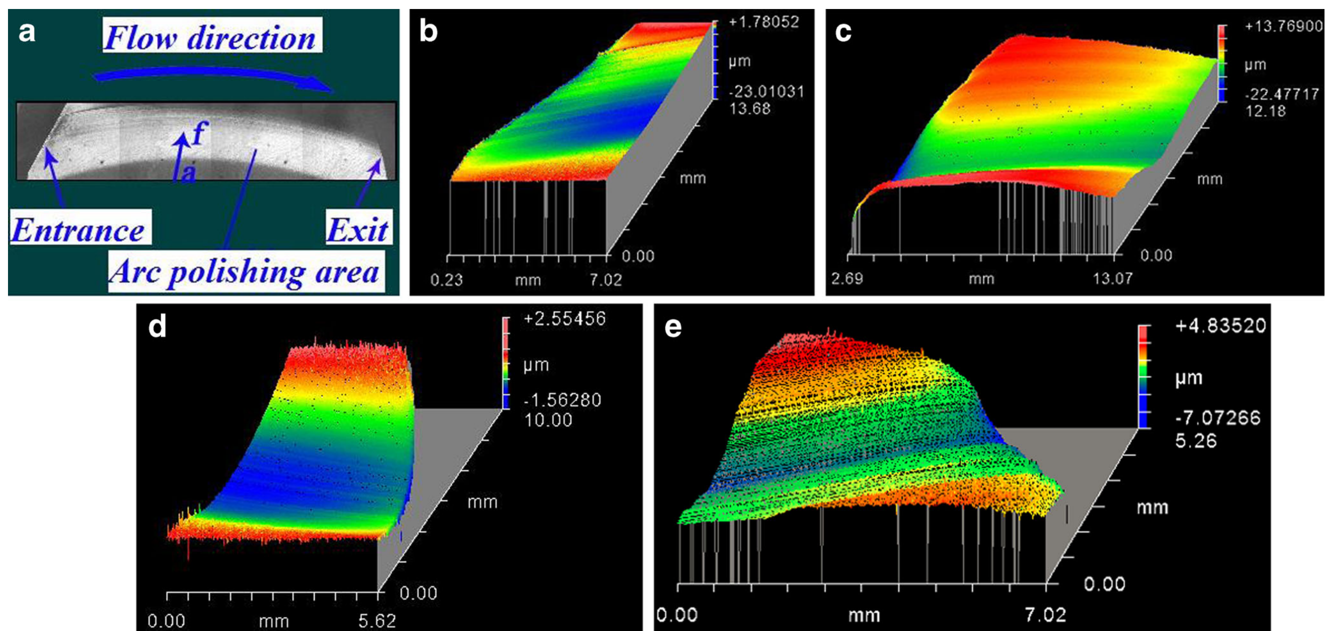

Fig. 6 Polishing belt of the monocrystalline 6H-SiC and Si wafer (magnets type: N35 cylindrical flat permanent magnets; magnets dimensions ϕ20 mm×15 mm; machining gap 0.8 mm; workpiece speed 0 rpm; polishing disk speed 200 rpm; process time 35 min). **a** Full morphology of arc polishing area, **b** 3D morphology of 6H-SiC at the entrance, **c** 3D morphology of Si at the entrance, **d** 3D morphology of 6H-SiC at the exit, and **e** 3D morphology of Si at the exit

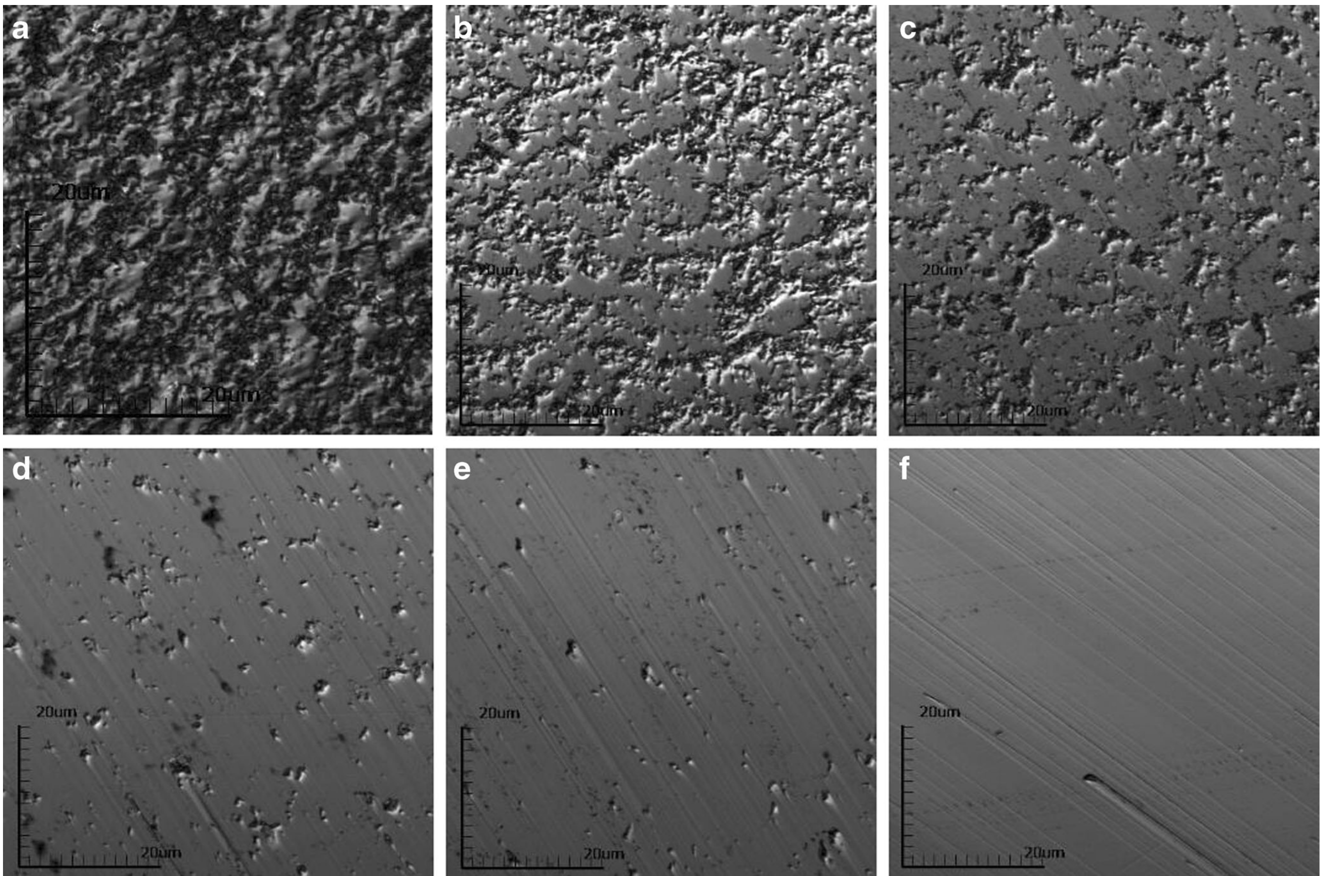

Fig. 7 **a**–**f** Radial morphology of different parts of the monocrystalline 6H-SiC wafer polishing area (magnets type: N35 cylindrical flat permanent magnets; magnets dimensions ϕ20 mm×15 mm; machining gap 0.8 mm; workpiece speed 0 rpm; polishing disk speed 200 rpm; process time 35 min)

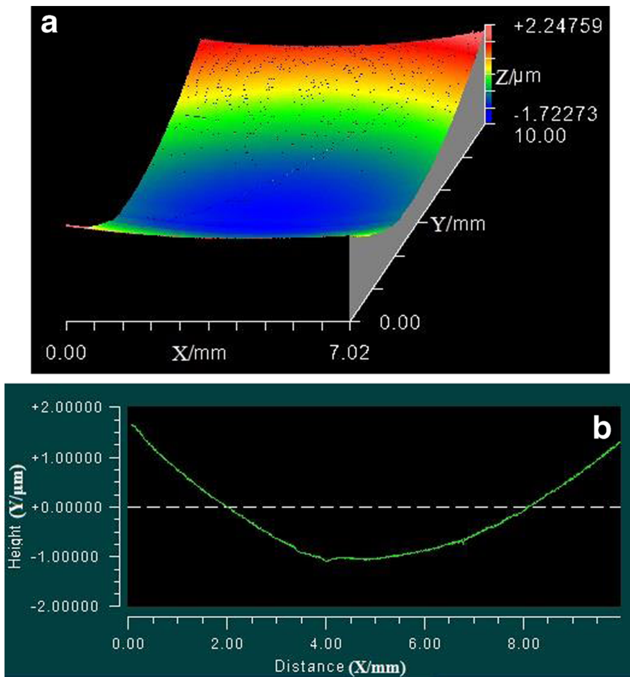

Fig. 8 Surface profile of polishing area. **a** 3D morphology of polishing ring and **b** surface profile of polishing belt cross section

monocrystalline Si wafer, both with diameter of 50.8 mm, were mounted on the workpiece clamping apparatus. By adjusting the *X*- and *Y*-axes, the wafer centre directly faced the pole centre. Through adjusting the Z-axis, the lower surface of the wafer was held at a distance of 0.8 mm from the upper surface of the polishing disk. Moreover, the workpiece is kept stable ($C2=0$), while the polishing disk rotates at $C1=$ 200 rpm. By running the apparatus for 35 min, an arc-shaped polishing belt was formed processed on the workpiece.

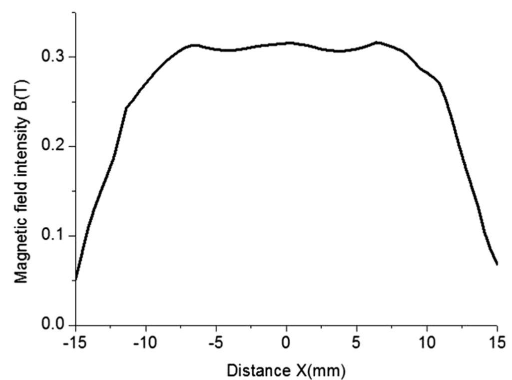

Fig. 9 Simulation result: magnetic field

Table 1 Simulation parameters

Parameter	Value	Parameter	Value
Workpiece diameter D (mm)	50.8	Vacuum permeability μ_0	1
Pole diameter d (mm)	20	Magnetic field intensity H (T)	Simulation value
Pole height h (mm)	15	The magnetoconductivity of magnetic particles μ	2000
Pole centre distance a (mm)	30	The proportion of magnetic particles in the MR fluid φ	0.33
Processing gap hr (mm)	0.8	The initial viscosity of the MR fluid η (Pa·s)	0.5
Speed of polishing disk v (m/s)	1.27	The rotational speed of work piece C1 n (rpm)	0
SiC hardness H_v (GPa)	38	Si hardness H_v (GPa)	12
SiC fracture toughness K_c (GPa)	1.9	Si fracture toughness K_c (GPa)	0.8
SiC elastic modulus E (GPa)	300	Si elastic modulus E (GPa)	170

3.2 Experimental results

3.2.1 Characteristics of polishing belt

Figure 6 shows the morphology of the polishing belt of the 6H-SiC wafer using a 3D optical surface profiler (NewView 7300). The material removal was relatively high at the entrance of the polishing belts on the surface of the monocrystalline 6H-SiC and Si wafers. On the entrance (when $x=0$), the material removal was the largest, and it gradually became smaller when approaching to the centre. These results suggested that the dynamic pressure generated by the micro-grinding head was maximised when it moved to $x=0$ and then reduced rapidly elsewhere. Moreover, the monocrystalline Si, with its lower hardness, owns a much higher material removal rate than monocrystalline 6H-SiC. This indicated that the properties of the workpiece material have the significant influences on the material removal (the correction coefficient described by Eq. (2)). The amount of material removal at the exit of the polishing belt was low and smooth for the monocrystalline 6H-SiC and Si wafers.

The morphology of the polishing belt of the monocrystalline 6H-SiC wafer along the a–f direction (Fig. 6a) can be seen in Fig. 7. Due to the magnetic intensity difference between the centre and the edge of the cylindrical magnetic poles, different MR pressures and abrasive fixity on different parts are generated (Eq. (4)). Therefore, material removal of the workpiece surface is varied. The region with larger volume of material removal becomes smoother, and the polishing belt is formed.

3.2.2 Material removal rate

Figure 8 shows the profile of the cross section of the polishing belt obtained by the surface profile function of the Zygo software. The profile of the polishing belt is similar to the cross section of the micro-grinding head (Fig. 2a). The centre of the polishing belt is corresponded to the centre of the micro-grinding head, and the maximum material removal rate can be obtained there.

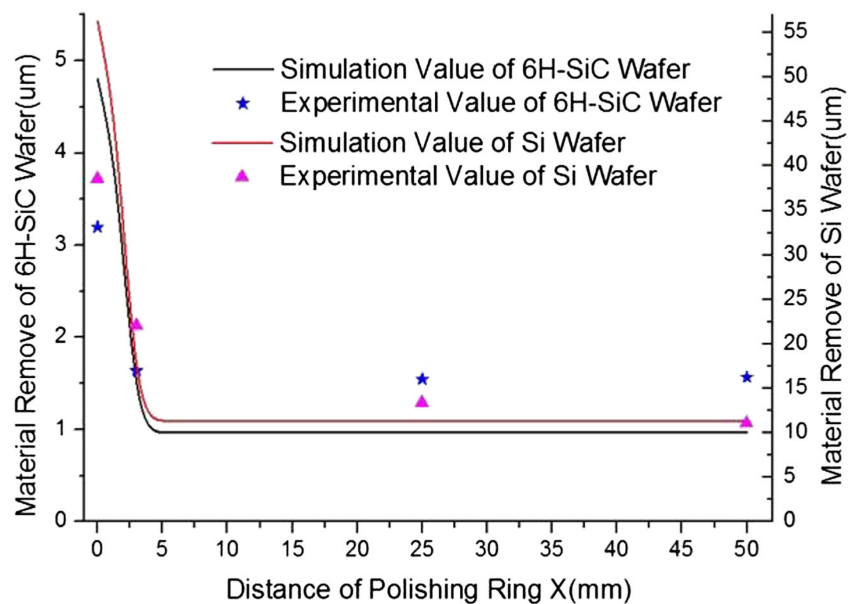

Fig. 10 Material removal characteristics

Figure 9 shows the magnetic field strength intensity of radial direction of the polishing head on the plane with the distance of 5.8 mm to the end surface of N35 cylindrical magnet (diameter 20 mm, height 15 mm) obtained by electromagnetic finite element analysis software Ansoft. By introducing the magnetic field strength intensity of the centre position and other parameters in Table 1 into Eq. (10), it is able to obtain the maximum material removal diagram curves of the polishing belts of the monocrystalline 6H-SiC and Si wafers (the β-curve was used for transition at points $X=0$ and $X>0$). Moreover, according to the cross section profile of the polishing belt, the maximum material removal of a polishing belt at different positions can be obtained. Finally, the material removal curve diagram of each polishing belt is drawn (see Fig. 10). The actual material removal is close to that simulated. Thus, the material removal model established by Eq. (10) is capable of quantitatively describing the material removal process of cluster MR material. In addition, the maximum material removal on the polishing belts of monocrystalline 6H-SiC and Si is 3.2 and 38.5 μm on the entrance, respectively. In other regions, it is 1.5 and 13.3 μm, respectively. By increasing the cluster magnetic pole density and the rotation and planar swing of the workpiece, polishing of large plane surface can be obtained in a short period [17, 18].

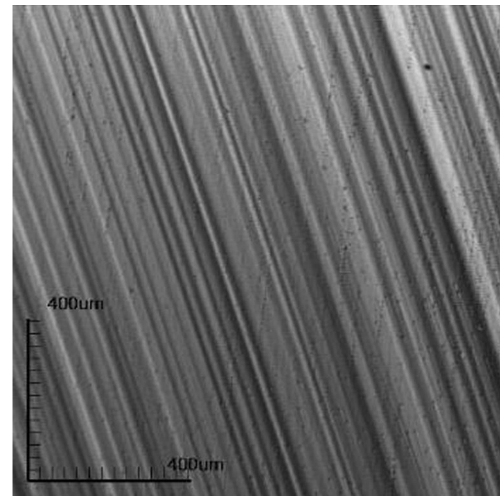

Fig. 12 Morphology of monocrystalline Si wafer

3.2.3 Material removal mechanism

Figure 11 shows the scanning electron microscope (SEM) images on the entrance and exit of the 6H-SiC wafer. As shown, there was a deep plastic removal groove on the entrance of the arc polishing belt. In particular, on the entrance ($x=0$), the groove depth was maximised. In the centre of the polishing belt, the groove depth is decreased. This means that there is the variation of dynamic pressure

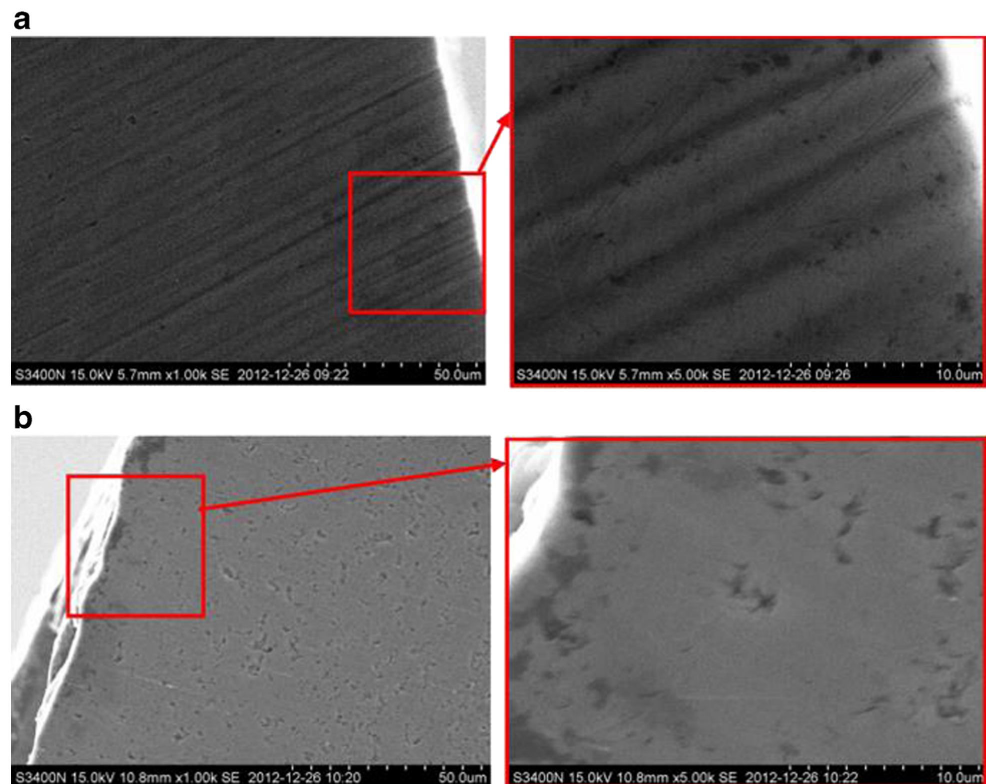

Fig. 11 SEM morphologies of monocrystalline 6H-SiC wafer polishing belt. **a** SEM morphology of the entrance and **b** SEM morphology of the exit

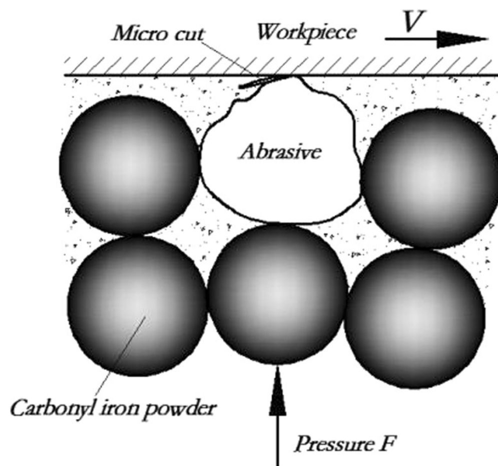

Fig. 13 Semi-fixed abrasive model of the micro-grinding head

from entrance to the centre. In contrast, grooves are not found on the exit of the polishing belt, and a smooth, flat surface with some pits and holes is identified. These pits and holes are possibly left from previous grinding processes. This means that with the decreasing of the dynamic pressure of the cluster MR fluid, the material removal rate is reduced.

Figure 12 shows confocal microscope images of the region near the entrance of the arc polishing belt of the monocrystalline Si wafer. Given constant conditions, the monocrystalline Si wafer owns deeper plastic removal grooves on the surface, even under low magnification microscopy. Deep plastic removal grooves are seen on the polishing belts of both materials, and the brittle material removal cannot be found.

The polishing pad constituted by the cluster MR micro-grinding head is formed by the magnetic chains distributed along the magnetic field lines. The densely arranged magnetic chains enabled the abrasive particles to be semi-fixed within the polishing pad through bonding, packing and clamping effects. Figure 13 shows the semi-fixed mode of action in this model of the abrasive. During the polishing, carbonyl iron powder that clamp abrasive particles would roll and slide as it contacts the workpiece surface (due to friction). The material on the workpiece surface is microscopically removed at a low rate during the mag-lev-induced rolling and sliding of the abrasives. When the magnetic field strength is large enough, the cutting effect of the abrasive on the workpiece appears, and the rolling and sliding effect of abrasives are reduced. However, the abrasives sink and lose material removal capacity due to the displacement and deformation of the carbonyl iron powder chain under the counteraction of the cutting force, which call the accommodated-sinking effect. Thus, the surface of workpiece is polished by the abrasives under elasto-plastic deformation. The subsurface damage induced by brittle removal can be avoided, and a damage-free, ultra-smooth surface can be obtained.

4 Conclusion

1. Based on the Preston equation, the variations of the dynamic pressure on the workpiece surface during the movement of a single micro-grinding head over a cluster MR membrane was investigated. A mathematical material removal model of cluster MR effect in plane polishing was established.
2. Arc polishing belts were processed on monocrystalline 6H-SiC and Si wafers, and the three-dimensional morphology of the polishing belts on both entrance and exit were analysed. For the polishing belts of monocrystalline 6H-SiC and Si, the maximum material removal is 3.2 and 38.5 μm in the entrance and 1.5 and 13.3 μm in other regions, respectively. By comparing the actual material removal of the polishing belt in different regions with a simulation result, the accuracy of the material removal model was verified.
3. Plastic removal grooves can be found on the polishing belts of SiC and Si wafers due to the semi-fixed abrasive and the elastico-plastic deformation of workpiece in cluster MR plane polishing. The subsurface damage induced by brittle removal can be avoided, and a damage-free, ultra-smooth surface can be obtained.

Acknowledgments The authors thank the National Natural Science Foundation of China (Grant nos 51305082, U1034006 and 51375097) for their financial support.

References

1. Kordonski W, Gorodkin S (2011) Material removal in magnetorheological finishing of optics. Appl Optics 50(14): 1984–1994. doi:10.1364/AO.50.001984
2. Miao C, Lambropoulos JC, Jacobs SD (2010) Process parameter effects on material removal in magnetorheological finishing of borosilicate glass. Appl Optics 49:1951–1963. doi:10.1364/AO.49.001951
3. Sidpara A, Jain VK (2012) Theoretical analysis of forces in magnetorheological fluid based finishing process. Int J Mech Sci 56(1):50–59. doi:10.1016/j.ijmecsci.2012.01.001
4. Sidpara A, Jain VK (2013) Analysis of forces on the freeform surface in magnetorheological fluid based finishing process. Int J Mach Tool Manu 69:1–10. doi:10.1016/j.ijmachtools.2013.02.004
5. Sidpara A, Jain VK (2011) Experimental investigations into forces during magnetorheological fluid based finishing process. Int J Mach Tool Manu 51(4):358–362. doi:10.1016/j.ijmachtools.2010.12.002
6. Sidpara A, Jain VK (2012) Nano level finishing of single crystal silicon blank using MRF process. Tribol Int 47:159–166. doi:10.1016/j.triboint.2011.10.008
7. Li YM, Shen XQ, Wang AL (2009) Nano-precision finishing technology based on magnetorheological finishing. Key Eng Mater 416:118–122. doi:10.4028/www.scientific.net/KEM.416.118
8. Degroote JE (2007)Surface interactions between nanodiamonds and glass in magnetorheological finishing (MRF). Dissertation, University of Rochester

9. Yin SH, Wang YQ, Deng GJ, Luo H, Chen FJ, Lu ZC (2013) Effects of permanent magnet excitation on material removal rate in area taking magnetorhelogical finishing. Adv Mater Res 2631(797):401–404. doi:10.4028/www.scientific.net/AMR.797.401
10. Shorey AB (2000) Mechanisms of material removal in magnetorheological finishing (MRF) of glass. Dissertation, University of Rochester
11. Niranjan M, Jha S, Kotnala RK (2014) Ball end magnetorheological finishing using bidisperse magnetorheological polishing fluid. Mater Manuf Process 29(4):487–492. doi:10.1080/10426914.2014.892609
12. Niranjan M, Jha S, Kotnala RK (2013) Mechanism of material removal in ball end magnetorheological finishing process. Wear 302(1–2):1180–1191. doi:10.1016/j.wear.2012.11.082
13. Jha S, Jain VK, Komanduri R (2007) Effect of extrusion pressure and number of finishing cycles on surface roughness in magnetorheological abrasive flow finishing (MRAFF) process. Int J Adv Manuf Techno 33(7):725–729. doi:10.1007/s00170-006-0502-x
14. Das M, Jain VK, Ghoshdastidar PS (2008) Analysis of magnetorheological abrasive flow finishing (MRAFF) process. Int J Adv Manuf Techno 38(5):613–621. doi:10.1007/s00170-007-1095-8
15. Guo HR, Wu YB, Lu D, Fujimoto M, Nomura M (2014) Effects of pressure and shear stress on material removal rate in ultra-fine polishing of optical glass with magnetic compound fluid slurry. J Mater Process Tech 214(11):2759–2769. doi:10.1016/j.jmatprotec.2014.06.014
16. Shimada K, Wu YB, Wong YC (2003) Effect of magnetic cluster and magnetic field on polishing using magnetic compound fluid (MCF). J Magn Magn Mater 262(2):242–247. doi:10.1016/S0304-8853(02)01497-X
17. Pan JS, Yan QS, Lu JB, Xu XP, Chen CK (2014) Cluster magnetorheological effect plane polishing technology. J Mech Eng 50(01):205–212. doi:10.3901/JME.2014.01.205
18. Pan JS, Yan QS, Xu XP, Tong HP, Zhu JT, Bai ZW (2013) Custer magnetorheological effect plane polishing on SiC single crystal slice. China Mech Eng 24(18):2495–2499. doi:10.3969/j.issn.1004-132X.2013.18.016
19. Wu ZC, Yan QS, Bai ZW, Kong LY, Chai JF (2011) Ultra smooth polishing research based on the cluster magnetorheological effect. Key Eng Mater 487:283–288. doi:10.4028/www.scientific.net/KEM.487.283
20. Yan QS, Gao WQ and Lu JB(2009) Grinding polishing method based on magnetic rheology effect and its polishing device. Patent, CN200610132495.9
21. Yang Y, Yan QS, Lu JB, Liu Y, Gao WQ (2009) Research on plane polishing using instantaneous tiny grinding wheel based on magnetorheological effect. Mach Tool & Hydra 37(12):5–7. doi:10.3969/j.issn.1001-3881.2009.12.002, **14**
22. Yi CJ (2011)Magnetorheological fluids: preparation, property and modeling. Dissertation, Chongqing University
23. Jha S, Jain VK (2006) Modeling and simulation of surface roughness in magnetorheological abrasive flow finishing (MRAFF) process. Wear 261:856–866. doi:10.1016/j.wear.2006.01.043
24. Luo JF (2011) Material removal mechanism in chemical mechanical polishing: theory and modeling. IEEE T SEMICONDUCT M 14(2):112–133. doi:10.1109/66.920723
25. Buijs M, Houten KKV (1993) Three-body abrasion of brittle materials as studied by lapping. Wear 166(2):237–245. doi:10.1016/0043-1648(93)90267-P
26. Buijs M, Houten KK-V (1993) A model for lapping of glass. J Mater Sci & Tech 28(11):3014–3020. doi:10.1007/BF00354706
27. Zhang F, Zhang XJ, Yu JC, Wang QT, Guo PJ (2000) Foundation of mathematics model of MR finishing. Optical Tech 26(02):190–192. doi:10.13741/j.cnki.11-1879/o4.2000.02.032
28. Yang PR (1998) Numerical analysis of fluid lubrication. Yang PR, Beijing